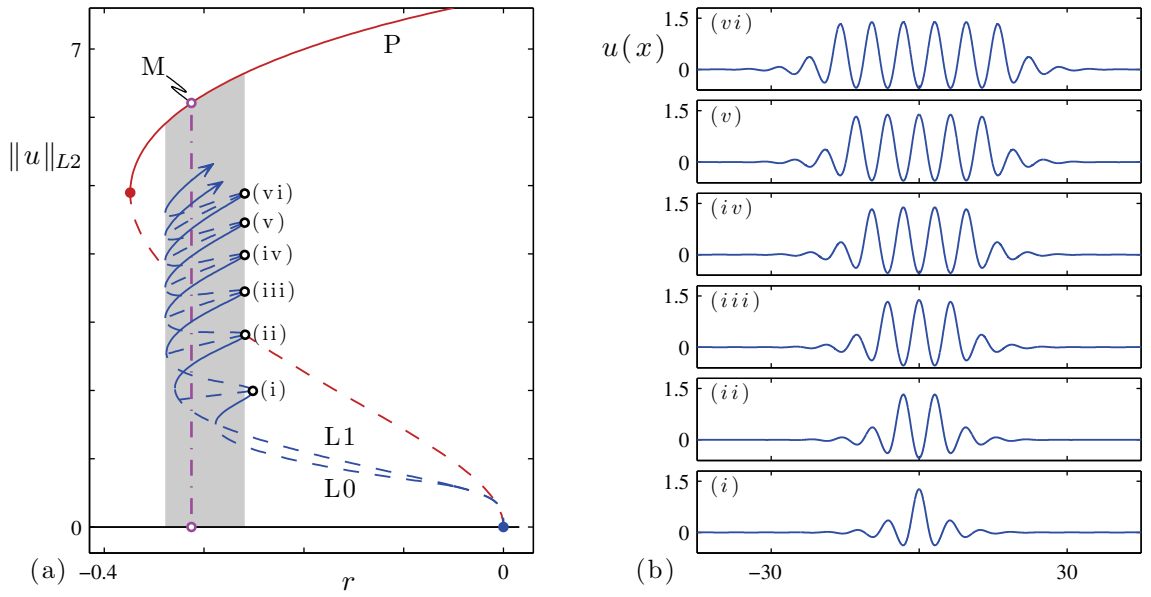

Figure 1. (a) *Bifurcation diagram of stationary solutions to* (1.1) *at* $b = 1.8$*, plotted in terms of the norm* $||u||_{L2} = (\int_\Omega u^2(x)dx)^{1/2}$*. Shading indicates the snaking region. The snaking branches* L0 *and* L1 *include even-symmetric localized states; the arrows indicate that on* $\Omega = \mathbb{R}$ *the snaking continues indefinitely. The rung branches which cross-link the snaking branches are also shown. The branch* P *of spatially periodic patterns satisfies* $H = 0$ *and includes the Maxwell point* M *at which* $\mathcal{F} = 0$*. The norm of solutions on* P *is rescaled so that this branch can be displayed on the same scale as the branches of localized states. Solid/dashed curves indicate stable/unstable solutions.* (b) *Profiles from several saddle-node bifurcations of the snaking branches; profiles* (i), (iii), *and* (v) *are from* L0*, and profiles* (ii), (iv), *and* (vi) *are from* L1*.*

and change stability at each saddle-node bifurcation; profiles from the segments of the snaking branches that slant "up and to the right" on the bifurcation digram in Figure 1 are stable, and those that slant "up and to the left" are unstable. All of the asymmetric profiles from the rungs are unstable.

The variational and conservative properties of the Swift–Hohenberg equation help considerably in understanding these localized states and the associated snaking bifurcation structure [7]. For example, the fact that the spatial dynamics associated with (1.1) is conservative determines the wavelength (i.e., the spatial period) of the pattern within the localized states. At fixed r, there typically exists an entire family of stationary, spatially periodic patterns $u_{\rm P}(x;k)$ parameterized by the wavenumber k. The particular pattern that is selected to appear within the localized state must lie in the level set $H = 0$. Figure 1 includes the branch P of spatially periodic states defined by $H = 0$, and the pattern wavenumber k varies with r along this branch to satisfy the $H = 0$ constraint. Careful measurement of the numerically computed localized states confirms that this branch of patterns correctly predicts the wavenumber variation $k(r)$ within the localized states, at least when the localized states are sufficiently wide. The variational property of (1.1) is also useful in understanding the localized states. The free energy $\mathcal{F}$ of the uniform-amplitude patterns varies along P. The so-called Maxwell point M is the r value at which the pattern on P has the same free energy as the

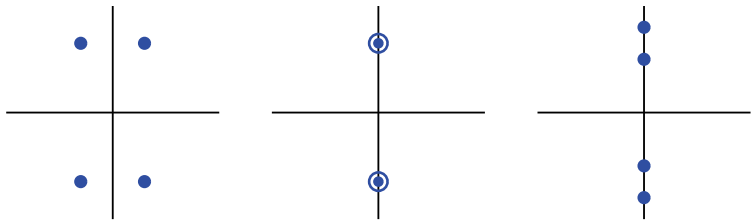

Figure 2. *Spatial eigenvalues of the trivial state $u = 0$ of the Swift–Hohenberg equation (1.1), plotted in the complex plane.* (a) *For $r < 0$ the eigenvalues form two complex conjugate nonreal pairs with real parts of equal magnitudes and opposite signs.* (b) *For $r = 0$ the eigenvalues are purely imaginary and of multiplicity two.* (c) *For $0 < r < 1$ the eigenvalues form two purely imaginary pairs. The same eigenvalue structure applies to the normal form of the Hamiltonian–Hopf bifurcation (2.1) in* (a) $\mu < 0$, (b) $\mu = 0$, *and* (c) $\mu > 0$.

enables us to establish the different regimes for the dynamics of this equation. Sections 3 and 4 contain numerical investigations of large-amplitude localized states far from onset. In section 3 we show that localized states in the extended Swift–Hohenberg equation (1.7) exhibit homoclinic snaking, though the details are not exactly the same as in the usual Swift–Hohenberg equation (1.1). In section 4 we examine the existence and stability of one-peak localized states. We find that there is both traveling wave ("drift") instability and standing wave instability of the single-peak state, and we discuss how these new bifurcations arise. Section 5 concludes.

2. Normal form coefficients.

In this section we use normal form analysis to examine the initial pattern-forming instability of the extended Swift–Hohenberg equation (1.7) at $r = 0$. The time-independent version of this equation forms a fourth-order spatial dynamical system. The four spatial eigenvalues of the fixed point associated with the trivial state $u = 0$ are given by $\{\pm(\sqrt{r} - 1)^{1/2}, \pm(-\sqrt{r} - 1)^{1/2}\}$. In $r < 0$ the four spatial eigenvalues form a complex quartet, and the origin is hyperbolic. At $r = 0$ the spatial eigenvalues collide pairwise on the imaginary axis, and in $0 < r < 1$ they form two imaginary pairs so that the origin is a center. Figure 2 shows the behavior in the spatial eigenvalues near $r = 0$, which is characteristic of the Hamiltonian–Hopf bifurcation. The dynamics in the normal form of this bifurcation are well understood, and the goal of this section is to classify the dynamics of the extended Swift–Hohenberg equation (1.7) by deriving the relationship between the coefficients in the normal form and the parameters in (1.7). A straightforward but lengthy method to determine this relationship is to explicitly transform the spatial dynamical system associated with (1.7) into normal form. This involves introducing a four-dimensional coordinate system which reproduces the spatial dynamics of (1.7) and then performing an appropriate linear transformation followed by a sequence of nonlinear near-identity transformations to match the normal form order by order. We choose an alternative method, based on [17] and later expanded in [6], which involves reducing (1.7) to an amplitude equation and comparing this to a suitable scaled reduction of the normal form. The values of the normal form coefficients in terms of the parameters from (1.7) can be read off by comparing the two reduced equations.

We begin in section 2.1 with a summary of the normal form for the Hamiltonian–Hopf

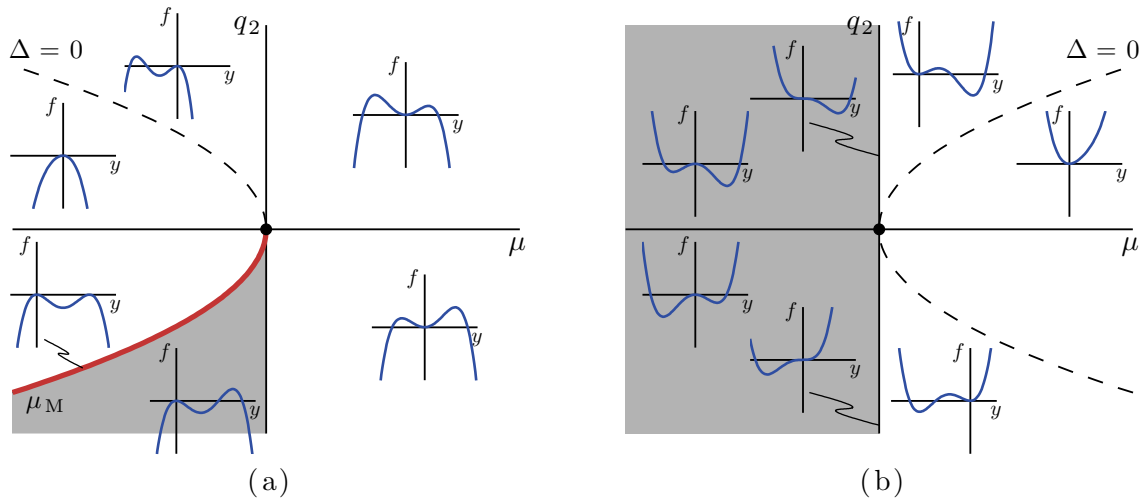

Figure 3. *Schematic summary of the regimes of normal form dynamics in the* (μ, q_2) *plane, in the cases* (a) $q_4 > 0$ *and* (b) $q_4 < 0$*, after Figures* 2 *and* 3 *of* [29]*. Orbits homoclinic to the origin exist in the shaded regions. The dashed curves indicate* $\Delta = 0$*, where the quantity* $\Delta \equiv q_2^2/4 + 4q_1q_4\mu/3$ *is the discriminant of* $f(y)/y^2$*. The solid line in* (a) *labeled* $\mu_{\rm M}$ *indicates the Maxwell point.*

where

$$f(y) = 4q_1\mu y^2 - 2q_2y^3 - \frac{4}{3}q_4y^4\,, \tag{2.4}$$

and by definition only $y \geq 0$ contains physically relevant solution trajectories.

Figure 3 indicates the shape of the potential function $f(y)$ for the different sign combinations of μ, q_2, and q_4. In the case $q_4 > 0$, Figure 3(a) shows that orbits homoclinic to the origin exist only in $q_2 < 0$ and only for $\mu_{\rm M} \leq \mu \leq 0$, where $\mu_{\rm M}$ is defined by the condition that the discriminant of $f(y)/y^2$ vanishes. At $\mu_{\rm M}$ the potential $f(y)$ has a doubly degenerate zero at a nontrivial value of y corresponding to a periodic orbit within the $w = h = 0$ level set; there is also a heteroclinic orbit (i.e., a spatial front) connecting the origin to this periodic state. The codimension-one point $\mu_{\rm M}$ is analogous to the Maxwell point in (1.1). While homoclinic orbits are certainly found throughout the shaded region in Figure 3(a), the multiplicity of localized states associated with homoclinic snaking is associated with the heteroclinic orbits along $\mu_{\rm M}$.

Turning to the case $q_4 < 0$, illustrated in Figure 3(b), we see that homoclinic orbits exist throughout $\mu < 0$ for q_2 of either sign. The homoclinic orbits for $q_2 < 0$ are born at small amplitude as μ decreases through zero, whereas the homoclinic orbits that exist near $\mu = 0$ when $q_2 > 0$ exist at finite amplitude. Moreover, exactly at $\mu = 0$ these homoclinic orbits have algebraically decaying tails since at $\mu = 0$ the origin is nonhyperbolic. In addition, Dias and Iooss [14] have shown that, for $q_4 < 0$ and in the regime where $\mu > 0$ and $q_2 > 0$, there exist orbits that are homoclinic to the periodic solutions.

2.2. Scaling the normal form. We wish to reduce the normal form (2.1) to an amplitude equation valid near the bifurcation at $\mu = 0$. The calculations that follow are simplified by

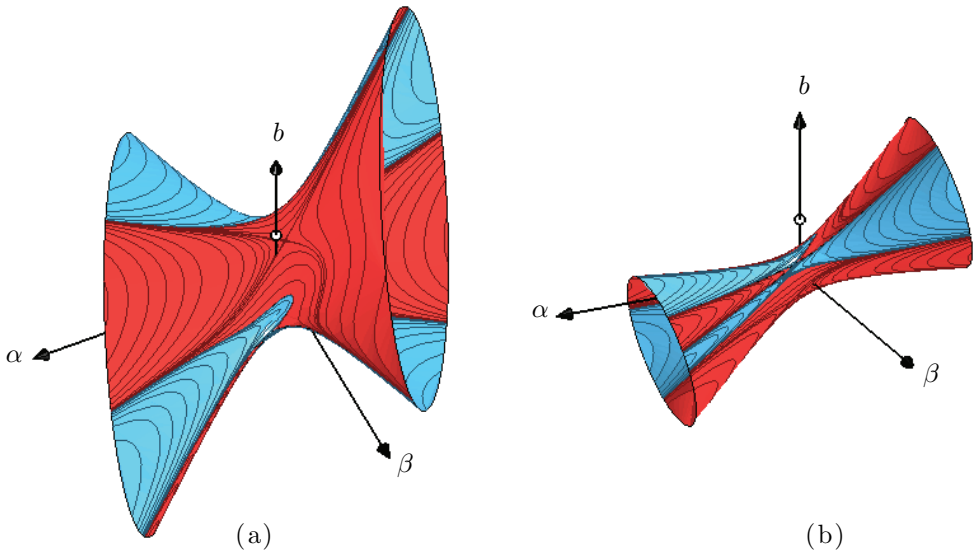

Figure 4. *Two views of the surface $q_2 = 0$ plotted in the $\mathbb{R}^3$ parameter space of the quadratic coefficients (b, α, β), with contours showing level sets of q_4. The surface is colored according to the value of q_4: Red and blue, respectively, correspond to positive and negative values of q_4. The open circle ($\circ$) marks the point $(b, \alpha, \beta) = (1.8, 0, 0)$. The surface can be viewed in the accompanying movie* 84397_01.mpg [local/web 5.98MB].

3. Homoclinic snaking in the extended Swift–Hohenberg equation. In this section we examine the behavior of localized states in the extended Swift–Hohenberg equation (1.7). The primary goal is simply to establish (numerically) that the homoclinic snaking behavior present in (1.1) persists with the inclusion of the nonvariational and nonconservative terms. We also point out several ways in which the localized states in (1.7) differ from those in (1.1). For simplicity, we fix $b = 1.8$ throughout this section and use the behavior of (1.1) at this value of b (as shown in Figure 1) as a point of reference. We make use of (2.20) to focus on values of the quadratic parameters (b, α, β) for which $q_2 < 0$ and $|q_2|$ is $\mathcal{O}(1)$—i.e., the highly subcritical regime, where homoclinic snaking is prominent—and we use the software package AUTO [15] to trace branches of localized states in the primary bifurcation parameter r.

To begin, we examine the effect of the new terms in (1.7) by increasing α from $\alpha = 0$ while leaving $\beta = 0$ fixed. Frames (a) and (b) of Figure 6 show the bifurcation diagrams of localized states at $\alpha = 0.1$ and $\alpha = 0.5$, respectively. The behavior of stationary, even-symmetric localized states is qualitatively the same as that shown in Figure 1 at $\alpha = 0$. These localized states are organized in a pair of intertwined snaking branches, which we continue to label L0 and L1. The saddle-node bifurcations on the snaking branches line up asymptotically (except perhaps the lowest two on the L0 branch) to two r values which define the snaking region. The shaded region in each frame indicates the snaking region at $\alpha = 0$, so increasing α increases the width of the snaking region and also shifts it to more negative values of r. Note, however, that in the case of (1.7) we cannot define a Maxwell point within this snaking region. Moreover, unlike in Figure 1, we do not indicate the stability of any localized states in Figure 6. A complete description of the stability of these states is beyond the scope of